The Role of Length and Defects on Optical Quantum Efficiency and Exciton Decay Dynamics in Single-Walled Carbon Nanotubes

D. Mark Harrah[†,‡,*] and Anna K. Swan[†,‡,§,*]

[†]Department of Electrical and Computer Engineering, [‡]Photonics Center, and [§]Department of Physics, Boston University, Boston, Massachusetts 02215

S ince the first measurements of photo-luminescence (PL) of single-walled carbon nanotubes,[1] the question of the intrinsic quantum efficiency has been explored. The initial estimate of the quantum efficiency was low, $\eta \sim 10^{-3}-10^{-4}$.[1,2] Recent advances in sample preparation methods[3,4] remove small bundles and produce nearly single chirality samples. Such samples have shown higher estimated intrinsic quantum efficiencies ($\sim$1%[5]), and samples with individual nanotubes have been even higher (2−8%[6−8]). The existence of a dark exciton level below the bright exciton band has been proposed as an explanation for low quantum efficiency.[9] Spataru *et al.* showed that this splitting has minimal effect at room temperature, and the more important effect is the thermal momentum blocking of the radiative transition.[10] The relatively low values of the quantum efficiency show that it is the nonradiative decay rate that dominates over the radiative decay rate. There are several nonradiative decay mechanisms proposed in the literature. At high fluences, exciton−exciton Auger de-excitation has been suggested.[11,12] Furthermore, excitons in doped semiconducting nanotubes can decay *via* electron−phonon interactions.[13] However, for undoped nanotubes in the linear regime, the main nonradiative decay mechanism is exciton diffusion to quenching sites, such as structural defects, adsorbate molecules, or the ends of the nanotube.[14−16] Stepwise fluorescence quenching in carbon nanotubes in response to changes to the nanotube's environment[16−18] can clearly also be utilized in sensor applications, such as biological sensors, ideally capable of detecting single molecules.[19]

ABSTRACT We perform Monte Carlo simulations of the time-resolved, spatially resolved, and integrated photoluminescence from a nanotube to investigate the role of the nanotube length L and defects using an exciton random-walk and defect-induced quenching model. When nonradiative decay is due solely to diffusion quenching, the quantum efficiency is approximately proportional to L^2 at low quantum efficiency. With defects present, the quantum efficiency depends only weakly on the number defects but is instead tied to L_{eff}^2 where L_{eff} is the root-mean-square separation between defects. The time-resolved photoluminescence decay of nanotubes is multiexponential for both pristine nanotubes and nanotubes with defects. The dominant time scale for a pristine nanotube is proportional to L^2/D, where D is the diffusion constant. The presence of defects on the nanotube introduces additional time scales.

The diffusion constant is the main parameter of the diffusion model, but it is not well-known. Experimentally extracted values of the diffusion constant range over 3 orders of magnitude, from 0.1 to 100 cm^2/s.[12,16,18,20,21] Environment, chirality variation, length distributions, sample quality, and the presence of bundling introduce complexities in the behavior of the optical properties of nanotubes. Therefore, it is important to first examine the expected behavior of an individual nanotube with well-controlled static or dynamic quenching defects as the only interaction with the environment.

In this paper, we assume that the observed diffusive behavior arises from random walks by excitons and perform Monte Carlo simulations of these random walks to model the fluorescence from nanotubes under uniform excitation (see Detailed Methods). From these simulations, we obtain the time-resolved, spatially resolved, and integrated quantum efficiency for nanotubes in the presence of perfectly quenching defects and of varying lengths. We show
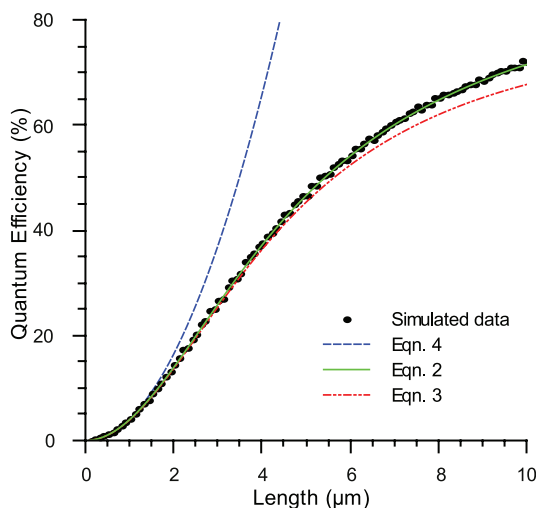
Figure 1. Simulated quantum efficiency *vs* nanotube length. The data are fit well by three terms of eq 2. The single-term approximation of eq 2 (that is, eq 3) underestimates the efficiency for long lengths. The quadratic approximation (eq 4) deviates from the data beyond 1.3 μm, where γ_r becomes comparable to γ_{nr}.

that diffusion analysis is valid (above a minimum length) and that a very simple approximation works well for short tubes. The diffusion coefficient $D = 20$ cm²/s, resulting from the pure dephasing time scale T_2^* and the exciton effective mass m^*, yields length-dependent exciton lifetimes that match experimentally measured time-resolved PL lifetimes of 20−60 ps.[15,22] Lastly, we discuss the expected influence of the environment and nanotube chirality on exciton dynamics.

RESULTS AND DISCUSSION

Dependence of Quantum Efficiency on Length. With diffusion-limited quenching as the dominant nonradiative decay mechanism, one expects a strong dependence on quantum efficiency with nanotube length.[23,24] Our simulation results for quantum efficiency *versus* length in Figure 1 show an initially quadratic increase in quantum efficiency with length that then saturates at longer lengths. The simulated process is strictly a random walk; however, when the distance between defects on the nanotube is much larger than the distance between interactions, the random walk may be treated as diffusion. Thus, the result can be approached analytically by considering diffusion on a fixed interval of length L with absorbing boundary conditions.[24] For a diffusion constant D, assuming the rates of other decay channels are much slower than diffusion-limited quenching, the probability that a diffusing particle has not decayed by time t is given by[25]

$$N(t) = \frac{8}{\pi^2} \sum_{n=1,3,5,\ldots} \frac{1}{n^2} e^{-n^2 \gamma_{nr} t} \qquad (1)$$

where $\gamma_{nr} = \pi^2 D / L^2$. For an effective radiative decay rate γ_r,[10] the quantum efficiency η is given by

$$\eta = \frac{8}{\pi^2} \sum_{n=1,3,5,\ldots} \frac{\gamma_r}{n^2(n^2 \gamma_{nr} + \gamma_r)} \qquad (2)$$

The n^2 factors ensure that the higher order terms quickly become negligible. Thus, the first term dominates and $N(t) \approx (8/\pi^2)e^{-\gamma_{nr}t}$. Hence, the quantum efficiency η can be approximated as

$$\eta \approx \frac{8}{\pi^2} \frac{\gamma_r}{\gamma_r + \gamma_{nr}} \qquad (3)$$

For thermal diffusion, the diffusion constant is determined by the thermal energy so that $D = (\tau kT)/(m^*)$. Here, kT is the thermal energy, m^* is the exciton effective mass, and τ is the mean free time between exciton−phonon scattering events. The diffusion constant can also be expressed in terms of mean square free path $\langle l^2 \rangle$: $D = \langle l^2 \rangle / 2\tau$. At room temperature ($T = 300$ K), with $m^* = 0.17$ m_e and $\tau = 75$ fs, the diffusion constant is $D = 20$ cm²/s, which gives a root-mean-square free path $\langle l^2 \rangle^{1/2} = (2D\tau)^{1/2} = 17.3$ nm. For this paper, we use $\gamma_r = 1$ ns⁻¹. See the Detailed Methods section for more information on these values. For $L = 1$ μm, the result of 4% quantum efficiency is comparable to measurements on individual nanotubes.[6−8]

An important transition point is when the nonradiative and radiative decay rates are equal. For $\gamma_r = 1$ ns⁻¹ and $D = 20$ cm²/s, this occurs when the nanotube is 4.4 μm in length. As the nanotube length approaches and increases above this value, decay from exciton quenching at the ends contributes less to the exciton's total lifetime, which approaches the effective radiative lifetime. Below this transition length, the overall lifetimes of excitons are predominantly determined by random walks to the ends of the nanotube (Figure 1).

For short nanotubes, $\gamma_r \ll \gamma_{nr}$ and so we have

$$\eta \approx \frac{8}{\pi^2} \frac{\gamma_r L^2}{\pi^2 D} \qquad (4)$$

Hence, for short nanotubes, $\eta \propto L^2$ with γ_r/D determining the constant factor. Extracting D from a measurement of efficiency as a function of nanotube length is then dependent on knowing γ_r. The quadratic approximation of eq 4 is shown in blue in Figure 1, agreeing with the simulated data up to 1.3 μm. At longer lengths, the approximation clearly breaks down.

Dependence of Quantum Efficiency on Defect Positions. We now explore how the quantum efficiency changes with the addition of fixed and transient extra defect positions. We simulate the quantum efficiency for different defect configurations for a 1 μm carbon nanotube under uniform illumination. In all configurations, the nanotube ends are considered to be fixed defects and zero, one, or two additional defects are added at different positions. For each defect configuration, 10 million exciton random walks are simulated and the numbers that end in radiative decay anywhere on the nanotube
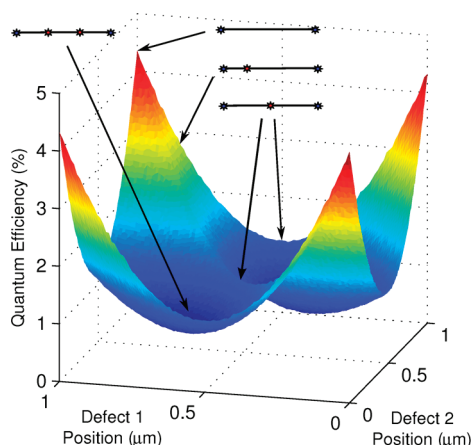
Figure 2. Simulated quantum efficiency for different defect configurations for a 1 μm nanotube. There are fixed defects at the ends of the nanotube and 0−2 additional defects with positions varying along the nanotube.

are counted. The percent that radiate, the quantum efficiency, is plotted in Figure 2 *versus* the position of the additional defects on the nanotube. The corners of the plot show the simulated quantum efficiency with only the two fixed defects at the ends of the nanotube. The edges and diagonal of the plot show the quantum efficiency of the nanotube with one additional defect as its position varies from one end to the other. The rest of the plot shows the quantum efficiency with two additional defects at different positions.

Figure 2 shows that there is not a well-defined value for the efficiency for one or two additional defects. Instead, there is a continuum of efficiencies depending on the position of the additional defects. In addition, the continuum of efficiencies for a single additional defect overlaps with the efficiences for two additional defects.

Hence, the addition of a defect to a nanotube results in a position-dependent change to the quantum efficiency. The minimum efficiency for both a single added defect and two added defects occurs when the defects are evenly spaced. On the other hand, when new defects are placed close to existing defects, the efficiency change is small.

In Figure 3, we plot quantum efficiency results (a) *versus* added defects and (b) *versus* root-mean-square (rms) defect-free length. It is immediately obvious that the rms length is a better measure of quantum efficiency than the extra number of defects. It means that the intensity measured in an experiment can be approximately related to the rms separation between defects.

This result can be understood analytically by considering multiple, perfectly quenching defects that split the nanotube into multiple, independent segments of length L_i. The quantum efficiency η_i of each segment i is given by $\eta_i \approx (8/\pi^2)(\gamma_r L_i^2/\pi^2 D)$. Weighting the efficiencies of the segments by the fraction of illumination each receives under uniform illumination gives the overall efficiency
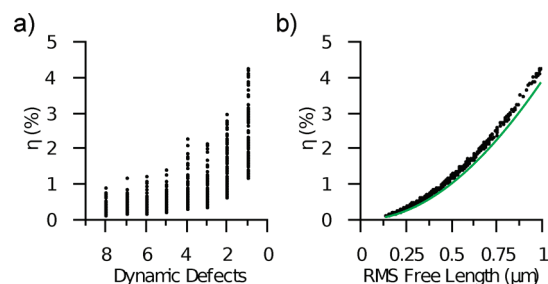

Figure 3. Simulated quantum efficiency η for a 1 μm nanotube: (a) η *vs* defect count; (b) η *vs* rms defect separation. The green line in (b) is eq 5 using $D = 20$ cm^2/s. The relation to rms defect separation correlates better than the relation to the number of defects.

$$\eta = \frac{\sum_i \eta_i L_i}{\sum_i L_i} \approx \frac{\gamma_r}{\pi^2 D} \frac{\sum_i L_i^3}{\sum_i L_i} = \frac{\gamma_r}{\pi^2 D} L_{\text{eff}}^2 \qquad (5)$$

where $L_{\text{eff}}^2 = (\sum_i L_i^3)/(\sum_i L_i)$ is the weighted mean square of the segment lengths. The expression in eq 5 only uses the first term in eq 1 and assumes that the length of the nanotube is such that nonradiative decay dominates radiative decay. It is therefore not an exact relation (Figure 3b).

In order to compare the quantum efficiency simulation to experimental results, we first consider time evolution of η for a single tube with quenchers attaching and detaching (stepwise quenching)[16,18] as is used for sensor applications.[19] We simulate the quantum efficiency of a nanotube as a function of time, with defects randomly created and destroyed on the nanotube. The nanotube also has permanent defects at specific intervals to mimic conditions for nanotubes embedded in a cross-linked polymer[17] or from defects induced during nanotube processing. In the simulation, the addi-
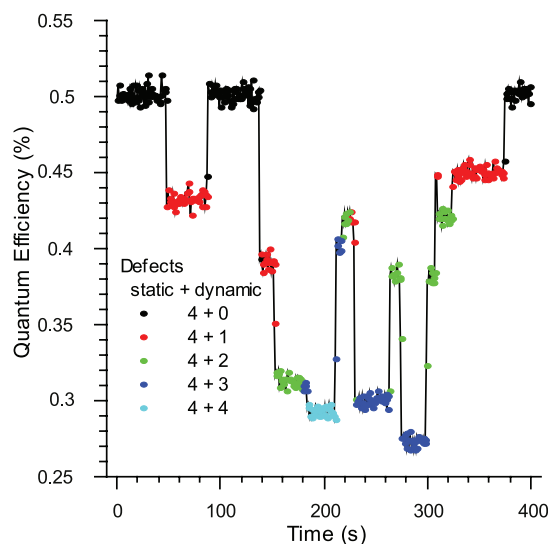

Figure 4. Simulated quantum efficiency for a 1 μm nanotube segment with fixed defects at 0.33 μm intervals and dynamic defects. The efficiency is color-coded by the number of defects on the nanotube.
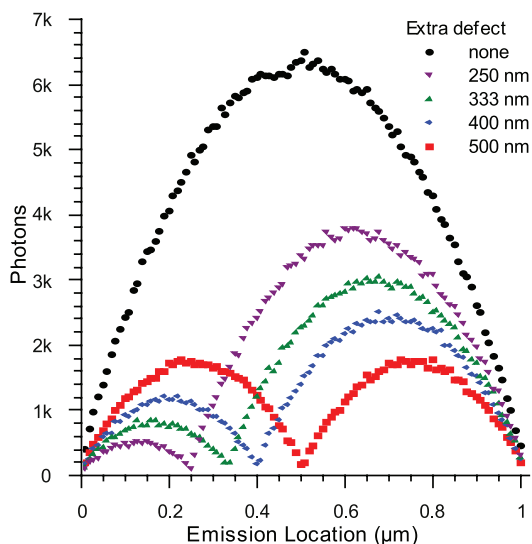
Figure 5. Spatial distribution of radiation with varying defect position for a 1 μm nanotube.

tional defects are created and destroyed at rates randomly selected from exponential probability distributions, and the position of a created defect is randomly selected from a uniform probability distribution.

The quantum efficiency is simulated for a 1 μm segment of nanotube with permanent defects at 0.33 μm intervals. The 1 μm segment corresponds to a diffraction-limited spatial bin in a representative experimental setup.[17] The simulated trace is shown in Figure 4 with the quantum efficiency color-coded by the number of defects on the nanotube for each simulated
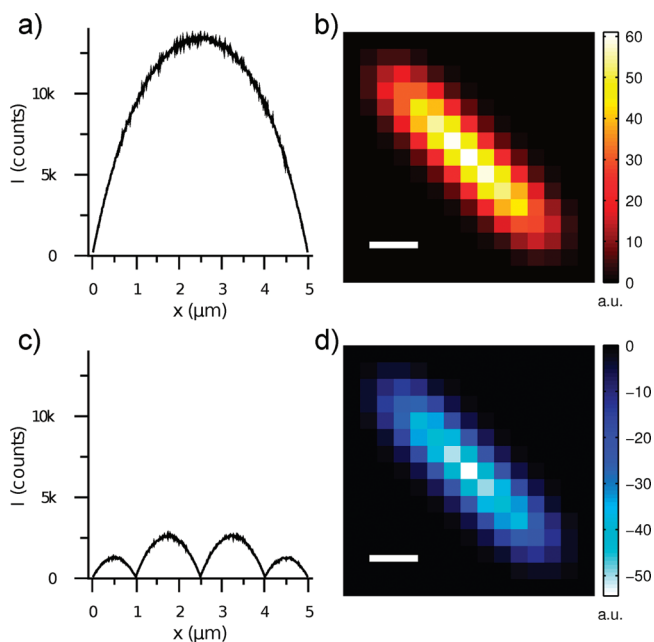

Figure 6. (a) Simulated spatial intensity profile from a 5 μm defect-free nanotube. (b) Simulated image of (a) for a Gaussian point spread function with fwhm = 785 nm and a 333 nm pixel size. (c) Simulated spatial intensity profile of the nanotube in (a) and (b), but with additional defects at 1, 2.5, and 4 μm. (d) Simulated image of intensity difference between (a) and (c). Parameters are as in (b). The scale bars are 3 pixels = 1 μm.

measurement. Each data point corresponds to the simulated fluorescence intensity integrated for 1 s generated by illumination that creates 1 million excitons/s uniformly over the entire segment. The fluctuations stem from the statistics of the events and do not include experimental sources of noise, such as shot noise or dark current.

The results show the typical steps observed in such experiments.[16−18] However, quantum efficiency and defect count are only weakly related, as also shown in Figure 3a. Rather, the quantum efficiency is a measure of how the rms defect-free length of the nanotube changes as a function of time.

Spatial Intensity Profile. If high-resolution imaging of the light emission is also used, such as tip-enhanced near-field[20,26,27] or localization,[28] information on the approximate origin of the emitted photons is captured. The simulation in Figure 5 shows the radiated photons for a nanotube length of 1 μm as a function of defect position on the nanotube. The intensity is zero at defects since they are perfect quenchers. With the same values as before (τ_r = 1 ns, m^* = 0.17 m_e, and τ = 75 fs, giving D = 20 cm^2/s), nonradiative decay dominates over radiative decay at any location on the nanotube.

Hence, the intensity does not saturate away from defects, and the distance between defects determines the exciton lifetime. Because diffusion determines the exciton lifetime, exciton excursion length is not a meaningful measure. We would see saturation of the signal between defects under a couple of different circumstances not considered here. We could introduce an additional, unspecified nonradiative decay channel faster than γ_{nr} = $(\pi^2 D)/(L^2)$. Similarly, if $\tau_r \ll \tau_{nr}$, which could be the case for lower D or shorter τ_r, the intensity would saturate away from defects.

By comparing the area under the curves, we can get an idea of the relative quantum efficiencies between different defect positions and for the different segments into which a defect divides a nanotube. As is expected from eq 5, the longest segment contributes the most.

The amount of detail in Figure 5 is not available for wide-field imaging. Figure 6, Figure 7, and Figure 8 demonstrate the image that would result with a Gaussian point spread function with full width at half-maximum (fwhm) 785 nm and a pixel size of 330 nm for different defect configurations.

These simulated images can help identify defect-free nanotubes from wide-field images. A defect-free nanotube will have a symmetric intensity profile, shown in Figure 6. A nanotube that has symmetrically positioned defects would also have a symmetric intensity profile, but other defect configurations would be asymmetric. From Figure 7, we see a random distribution of defects that is clearly asymmetric. The uniformly spaced defects in Figure 8, however, retain symmetry. This configuration demonstrates that, for a nanotube with de-

fects spaced below the diffraction limit, the defects contribute to a near-constant intensity over the length of the nanotube in contrast to the peaked curve in Figure 6a. An additional defect will create a point-like change in the intensity because it can only affect the intensity from a segment of the nanotube below the diffraction limit.

The longest defect-free segment dominates the intensity profile. This is clear in the randomly spaced defect configuration in Figure 7. The nanotube is twice as long as this segment, but the segment provides nearly all of the nanotube's intensity. As demonstrated in the figure, an additional defect will have a much greater effect if it is created in this segment than elsewhere on the nanotube.

Exciton Dynamics and Time-Resolved Photoluminescence. We next consider the case of the exciton decay dynamics for a pristine nanotube with only end defects. The nonradiative decay is solely due to quenching at the end defects, which are assumed to be perfectly quenching as before. From eq 1, we expect a multiexponential decay. The time constants involved have the form $\tau_{nr}, \tau_{nr}/9, \tau_{nr}/25, ..., \tau_{nr}/n^2$ for odd n. The higher order, faster decay terms have reduced amplitudes, so the decay is predominantly due to a single exponential at longer times. The faster decay components are only relevant at shorter times.

The characteristic nonradiative decay time for a nanotube of length L and diffusion constant D is $\tau_{nr} \approx L^2/(\pi^2 D)$. For a 1 μm nanotube with $D = 20$ cm^2/s, this gives $\tau_{nr} = 51$ ps. This is much less than the radiative lifetime of 1 ns that we have been assuming. So, for a single segment of length L, the decay dynamics are dominated by diffusion in an interval with absorbing boundary conditions. To first order, $N(t) \approx e^{-t/\tau_{nr}}$. Hence, we note that the (dominant) decay rate for nanotubes of the same chirality will differ due to variations in length and that, for time-resolved measurements with picosecond resolution, the decay will likely appear as monoexponential decay.

The simulated photoluminescence from a 1 μm nanotube as a function of time is shown in Figure 9. In addition, the calculated photoluminescence is plotted using the first 1 to 4 terms of eq 1. A single exponential fits well after about 10 ps. A second term improves the agreement at shorter times, and at four terms, there is no noticeable discrepancy. Note that a general biexponential, which has unconstrained amplitudes and rates, can fit the plotted range fairly well in practice. The slower rate obtained from such a fit is usually close to the first order time constant τ_{nr}. The faster rate accounts for several higher order terms in eq 1 and is not directly meaningful.

We compare these results with a previous timeresolved study on single individual nanotubes.[22] They find that nanotubes with the same chirality exhibit a variation of decay times between 28 and 66 ps. Assum-
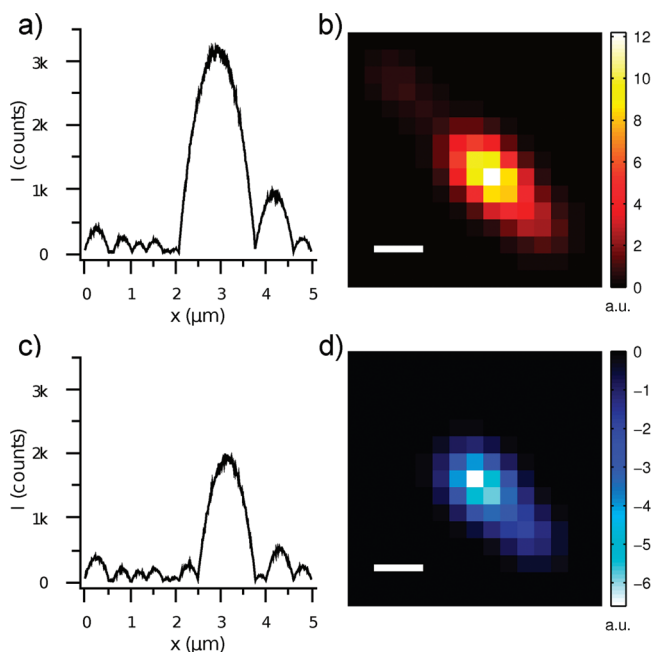

Figure 7. (a) Simulated spatial intensity profile from a 5 μm nanotube with random defect sites at an average interval of 400 nm according to an exponential probability distribution. (b) Simulated image of (a) for a Gaussian point spread function with fwhm = 785 nm and a 333 nm pixel size. (c) Simulated spatial intensity profile of the nanotube in (a), but with additional defects at 1, 2.5, and 4 μm. (d) Simulated image of intensity difference between (a) and (c). Parameters are as in (b). The scale bars are 3 pixels = 1 μm.

ing pristine nanotubes, this range would correspond to a length variation of 0.74 to 1.1 μm according to the diffusion model with $D = 20$ cm^2/s. They also find a much slower decay rate that they associate with a dark exciton band with a time constant that is between 155 and 330 ps. The longer time constant for dark excitons is in accordance with a heavier effective mass for the lowest dark exciton[29] that will result in a slower diffusion rate.

Introducing defects to the nanotube will change the exciton dynamics considerably. Figure 10 shows the radiation as a function of time for a 3 μm nanotube with defects at the ends and at 0.6 and 1.5 μm. Each segment between defects can be treated separately, and so the radiation at a specific time is the sum of the radiation from each segment, weighted appropriately for the fraction of illumination each receives. The characteristic nonradiative decay time for each segment is $\tau_{nr,i} \approx L_i^2/(\pi^2 D)$. For the 0.6, 0.9, and 1.5 μm segment lengths here, the first order lifetimes are 18, 41, and 114 ps. The decay curve for the entire nanotube is thus more strongly multiexponential than for a single length.

Figure 11 compares the exciton decay curves from nanotubes with end defects and one additional defect. If the additional defect is placed in the middle, the nanotube is broken into two identical segments. The decay is predominantly monoexponential for longer times since there is only one length scale involved. As
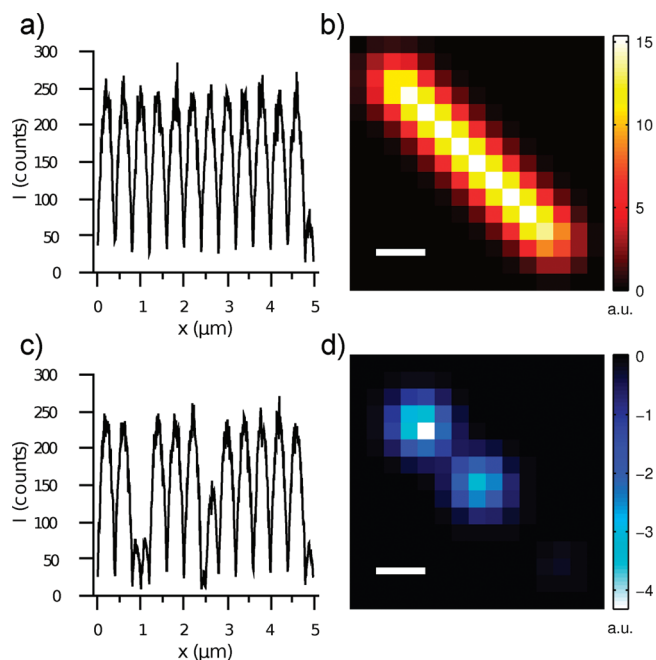
Figure 8. (a) Simulated spatial intensity profile of a 5 μm nanotube with defects at constant 400 nm intervals. (b) Simulated image of (a) for a Gaussian point spread function with fwhm = 785 nm and a 333 nm pixel size. (c) Simulated spatial intensity profile of the nanotube in (a), but with additional defects at 1, 2.5, and 4 μm. (d) Simulated image of intensity difference between (a) and (c). Parameters are as in (b). The scale bars are 3 pixels = 1 μm.

in Figure 9, a faster rate does show up at short time scales. Other defect positions show a stronger multiexponential behavior because of different decay rates from two length scales. As the defect position moves close to the end, most of the radiation comes from the larger segment and the decay returns to being mostly monoexponential. Hence, predominantly monoexponential decay dynamics is one indicator of a defect-free
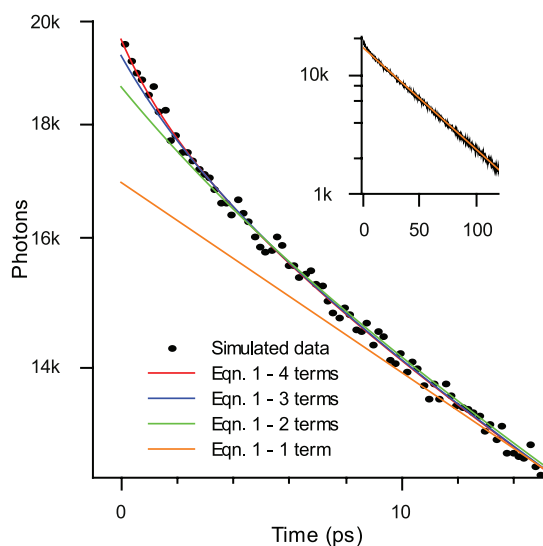

Figure 9. Black points: simulated PL for a 1 μm nanotube with end defects only. Lines: calculated curves using the first 1 to 4 terms of eq 1. The higher order terms account for the faster decay at short times. Inset: decay is predominantly monoexponential at longer times.

nanotube. A nanotube with defects can only have predominantly monoexponential decay if its defects are nearly uniformly spaced or the defects are close to the ends of the nanotube.

To analyze the time-resolved exciton decay for an ensemble of nanotubes, eq 1 must be averaged over a distribution of defect-free lengths $P(L)$. The exciton population for the ensemble is then $\tilde{N}(t) = \int_0^\infty P(L) N(t, L) \mathrm{d}L$, where $N(t, L)$ explicitly indicates the length dependence in eq 1. A common length distribution is the exponential distribution $P(L) = \rho e^{-\rho L}$, which describes uniformly random defects with average density ρ. In this case, the population decay is a stretched exponential:[25] $\tilde{N}(t) \propto e^{-\rho(8Dt/\pi)^{1/2}}$. However, the exponential length distribution is not strictly applicable in practice because there is an underlying length distribution of the nanotubes themselves. Prior knowledge of this length distribution may be required in order to accurately extract the desired physical parameters ρ and D.[30]

Below nanotube lengths of 500 nm, the diffusion approximation of the random walk model used in this paper starts to break down. This is initially apparent in the time-resolved data, such as in Figure 11, where the shortest length scale is 250 nm. Because of this, the simulated data in Figure 11 is fit to eq 1 instead of directly plotting eq 1. The obtained D from this fit is length-scale-dependent and slightly smaller than in the limit where D is constant. For the nanotube with a defect at 250 nm, we obtain 17.6 cm²/s for the shorter segment and 19 cm²/s for the longer segment instead of the expected 20 cm²/s. When the segment lengths are at least 1 μm, the obtained D is 20 cm²/s as expected.

Influences on Diffusion Constant. Local potential variations in the nanotube's environment will modify the exciton velocity distribution and produce a spatially varying diffusion constant. This could trap an exciton in a segment of the nanotube away from defects.[31] The nonradiative decay rate would decrease and thus the quantum efficiency would increase. Hence, we would expect a nanotube suspended in air to have a different diffusion constant from a nanotube on a surface or in a medium.[18,21,32] In the context of a sensor, local trapping would decrease the absolute change in the nanotube's fluorescence in response to defects. It would, however, increase the range of the sensor and provide better correlation between the number of defects on the nanotube and the fluorescence intensity.

Here we have only considered the dynamics and quantum efficiency at constant temperature. As the temperature is lowered, the diffusion constant itself is affected since τ increases[33,34] while kT decreases. The temperature dependence of the quantum efficiency is more complex. The thermal population of the bright state will decrease at very low temperature.[10,35,36] On the other hand, the effective radiative lifetime will de-
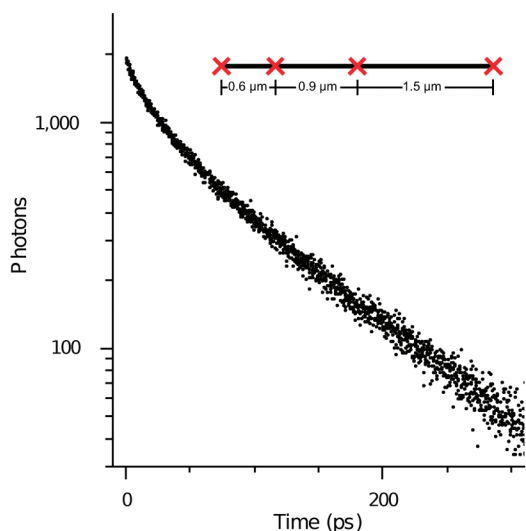
Figure 10. Simulated time-resolved PL from a 3 μm nanotube with quenching defects at 0, 0.6, 1.5, and 3 μm showing multiexponential decay.

Figure 12. Simulated quantum efficiency *vs* nanotube length for different random walk parameters. The black squares plot the dependence on length for the parameters used in this paper ($D = 20$ cm²/s). The green circles show the length dependence for a faster dephasing time, which gives a smaller diffusion constant $D = 2$ cm²/s. The red triangles show the dependence for a smaller effective mass, which corresponds to a larger diffusion constant $D = 200$ cm²/s.

crease and then increase[10,29] in addition to changes in the nonradiative rate due to diffusion.

The properties that influence the diffusion constant also vary by nanotube chirality. This causes corresponding variations in the quantum efficiency according to the diffusion model. For example, the effective mass of an exciton differs noticeably between chiralities.[37] Because the diffusion constant is inversely proportional to the effective mass, differences in effective mass translate into different nonradiative decay rates and, thus, quantum efficiencies. Similarly, variations in the effective radiative lifetime or phonon interaction times across chiralities
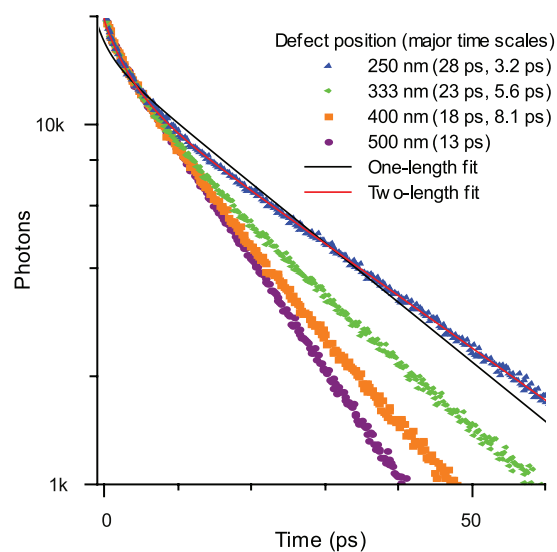
will directly produce corresponding variations in the quantum efficiency. Figure 12 shows the effect of these variations on the length dependence of the quantum efficiency of the nanotube.

CONCLUSION

We consider a model of exciton decay where nonradiative decay is due to random walks to quenching sites. In the diffusion limit, the quantum efficiency η is determined by the diffusion constant D, radiative decay rate γ_r, and the defect configuration. For a short, pristine nanotube, the quantum efficiency is approximately $\eta \approx (8/\pi^2)(\gamma_r L^2/\pi^2 D)$. The corresponding nonradiative decay rate is $\gamma_{nr} = \pi^2 D/L^2$. For a nanotube with defects, the defect configuration can be approximated at shorter lengths by an effective length L_{eff}, where L_{eff} is the root-mean-square of the distance between defects. The quantum efficiency is then $\eta \approx (8/\pi^2)(\gamma_r L_{eff}^2)/(\pi^2 D)$. The effective length correlates better with the quantum efficiency than the defect count.

The simulations of wide-field images of nanotubes illustrate how the spatial intensity profile of nanotubes is affected by defects. The intensity of defect-free nanotubes are symmetric, with a single peak in the center that decreases monotonically toward the ends. A nanotube with a uniform intensity profile has defects spaced at distances below the diffraction limit of the imaging system. The intensity change caused by an additional defect is greatly affected by the length of the defect-free segment to which it attaches and the position within that segment.

The exciton decay dynamics due to the random-walk model are multiexponential for two different

Figure 11. Radiation *vs* time for a 1 μm nanotube with defects at the ends and a single extra defect at different positions. A shorter rms defect separation implies a faster decay rate. Defects close to the ends do not modify the rms separation much and so have less effect on the decay rate. The lines fit the radiation from a nanotube with a defect at 250 nm with eq 1 using a single length (black) and two lengths (red).
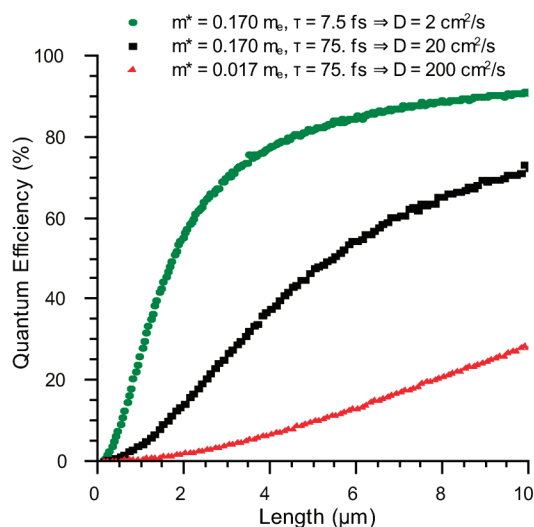
reasons. First, for a pristine nanotube with the ends considered as defects, exciton decay can be considered as diffusion on an interval with absorbing boundaries. The resulting formula for exciton population as a function of time is intrinsically a sum of exponentials with decreasing amplitude and lifetime. Second, a nanotube may have defects, which divide the nanotube into multiple, independent segments with different lengths. Each length contributes a different series of lifetimes to the exciton decay curve.

The existence of defects on a nanotube is most clearly manifested in time-resolved measurements. A defect-free nanotube will have an exciton population that decays predominantly monoexponentially (apart from a much slower dark exciton band diffusion not considered here) with higher order components on the order of 1 ps for the values used in this paper.

DETAILED METHODS

The simulations model the dynamics of excitons in single-walled carbon nanotubes according to several fundamental assumptions. An exciton decays to E_{11} quickly, and so diffusion is only considered in E_{11}. The exciton is strongly localized axially and thus can be treated as a one-dimensional classical particle. An exciton randomly walks the nanotube by rethermalizing (obtaining a new velocity based on a thermal distribution) on some characteristic time scale. We take the exciton dephasing time as a conservative, short estimate of this time. Nonradiative decay is due to perfectly annihilating defects and nanotube ends.[17,38] An exciton within half of the effective exciton size of a defect or end is assumed to decay nonradiatively immediately. Uniform illumination of the nanotube is assumed, so that the exciton starting position is uniformly distributed along the nanotube. Exciton−exciton annihilation is not considered, so each exciton can be simulated independently. This is a reasonable assumption for typical continuous wave illumination intensities.[16,18]

The actual simulation of an individual exciton's random walk is event-based. This means that rather than computing the system state at fixed time intervals, the simulation determines the time that the next event that will occur and propagates the system to that time. The first event in the simulation is exciton creation. At creation, the exciton's initial position along the nanotube is randomly selected with all positions equally probable. The exciton gets an initial velocity according to a thermal distribution and a radiative lifetime according to an exponential probability distribution with average τ_r. The thermal distribution is parametrized by the effective mass of the exciton and the temperature of the nanotube. The exciton is also given a random time after which it will rethermalize. When an exciton rethermalizes, it gets a new velocity and a new rethermalization time. The rethermalization time is randomly selected according to an exponential probability distribution with average τ.

The simulation proceeds by determining the next event that will occur. The possible events are radiative decay, nonradiative decay, or rethermalization. The time at which each of these events would occur is calculated and the event occurring at the earliest time is selected. The time at which radiative decay would occur is fixed by the exciton's radiative lifetime, which was randomly selected at its creation. For nonradiative decay, the event time is determined by the exciton's current velocity and distance to the nearest defect along its direction of travel. The time at which rethermalization will occur is fixed by the time randomly selected at the previous rethermalization event or at the creation of the exciton if there has not yet been a rethermalization event.

If the next event is decay, the time and position at which it occurs is recorded as the exciton's actual lifetime and final position, respectively. The type of decay, radiative or nonradiative, is recorded, and the simulation of that exciton is complete. If the event is a rethermalization event, the exciton moves to its new position. It then gets a new randomly selected velocity and a new randomly selected time at which it will rethermalize. The process repeats until the exciton decays. In the diffusion limit, many rethermalization events precede the final decay event. In the ballistic limit, almost all events are radiative or nonradiative decay and there are few rethermalizations.

The external values that enter into the simulations are the average time between scattering events τ, the exciton effective mass, m^*, the effective radiative lifetime[10] τ_r, exciton size, and the nanotube temperature T. The choice of τ is based on T_2^*, the pure dephasing time. T_2^* has been measured as $70-160$ fs at low fluence both by time-domain measurement[34,39] and frequency-domain measurement of the E_{11} homogeneous line width.[16,6] Here we use the lower limit $\tau = 75$ fs, which corresponds to the lower range of the diffusion constant. The exciton effective mass used is 0.17 m_e, which is the tight-binding value calculated for a (6,5) nanotube.[37] For the parameters described here, an exciton random walk in the diffusion limit would have a diffusion constant of 20 cm^2/s. The effective radiative lifetime for each exciton is taken to be on average 1 ns[29,40] and the size of the exciton is 2 nm.[12,41,42] We use room temperature, 300 K, for the temperature of the nanotube.

REFERENCES AND NOTES

1. O'Connell, M. J.; Bachilo, S. M.; Huffman, C. B.; Moore, V. C.; Strano, M. S.; Haroz, E. H.; Rialon, K. L.; Boul, P. J.; Noon, W. H.; Kittrell, C.; *et al.* Band Gap Fluorescence from Individual Single-Walled Carbon Nanotubes. *Science* **2002**, *297*, 593–596.
2. Wang, F.; Dukovic, G.; Brus, L. E.; Heinz, T. F. Time-Resolved Fluorescence of Carbon Nanotubes and Its Implication for Radiative Lifetimes. *Phys. Rev. Lett.* **2004**, *92*, 177401.
3. Arnold, M. S.; Green, A. A.; Hulvat, J. F.; Stupp, S. I.; Hersam, M. C. Sorting Carbon Nanotubes by Electronic Structure Using Density Differentiation. *Nat. Nanotechnol.* **2006**, *1*, 60–65.
4. Tu, X.; Manohar, S.; Jagota, A.; Zheng, M. DNA Sequence Motifs for Structure-Specific Recognition and Separation of Carbon Nanotubes. *Nature* **2009**, *460*, 250–253.
5. Crochet, J.; Clemens, M.; Hertel, T. Quantum Yield Heterogeneities of Aqueous Single-Wall Carbon Nanotube Suspensions. *J. Am. Chem. Soc.* **2007**, *129*, 8058–8059.
6. Lefebvre, J.; Austing, D. G.; Bond, J.; Finnie, P. Photoluminescence Imaging of Suspended Single-Walled Carbon Nanotubes. *Nano Lett.* **2006**, *6*, 1603–1608.
7. Tsyboulski, D. A.; Rocha, J.-D. R.; Bachilo, S. M.; Cognet, L.; Weisman, R. B. Structure-Dependent Fluorescence Efficiencies of Individual Single-Walled Carbon Nanotubes. *Nano Lett.* **2007**, *7*, 3080–3085.
8. Carlson, L. J.; Maccagnano, S. E.; Zheng, M.; Silcox, J.; Krauss, T. D. Fluorescence Efficiency of Individual Carbon Nanotubes. *Nano Lett.* **2007**, *7*, 3698–3703.
9. Zhao, H.; Mazumdar, S. Electron-Electron In-teraction Effects on the Optical Excitations of Semiconducting Single-Walled Carbon Nanotubes. *Phys. Rev. Lett.* **2004**, *93*, 157402.
10. Spataru, C. D.; Ismail-Beigi, S.; Capaz, R. B.; Louie, S. G. Theory and *Ab Initio* Calculation of Radiative Lifetime of Excitons in Semiconducting Carbon Nanotubes. *Phys. Rev. Lett.* **2005**, *95*, 247402.
11. Ma, Y.-Z.; Valkunas, L.; Dexheimer, S. L.; Bachilo, S. M.; Fleming, G. R. Femtosecond Spectroscopy of Optical Excitations in Single-Walled Carbon Nanotubes: Evidence

for Exciton−Exciton Annihilation. *Phys. Rev. Lett.* **2005**, *94*, 157402.

12. Lüer, L.; Hoseinkhani, S.; Polli, D.; Crochet, J.; Hertel, T.; Lanzani, G. Size and Mobility of Excitons in (6,5) Carbon Nanotubes. *Nat. Phys.* **2009**, *5*, 54–58.

13. Perebeinos, V.; Avouris, P. Phonon and Electronic Nonradiative Decay Mechanisms of Excitons in Carbon Nanotubes. *Phys. Rev. Lett.* **2008**, *101*, 057401.

14. Korovyanko, O. J.; Sheng, C.-X.; Vardeny, Z. V.; Dalton, A. B.; Baughman, R. H. Ultrafast Spectroscopy of Excitons in Single-Walled Carbon Nanotubes. *Phys. Rev. Lett.* **2004**, *92*, 017403.

15. Hagen, A.; Steiner, M.; Raschke, M. B.; Lienau, C.; Hertel, T.; Meixner, A. J.; Hartschuh, A. Exponential Decay Lifetimes of Excitons in Individual Single-Walled Carbon Nanotubes. *Phys. Rev. Lett.* **2005**, *95*, 197401.

16. Cognet, L.; Tsyboulski, D.; Rocha, J.-D. R.; Doyle, C. D.; Tour, J. M.; Weisman, R. B. Stepwise Quenching of Exciton Fluorescence in Carbon Nanotubes by Single-Molecule Reactions. *Science* **2007**, *316*, 1465.

17. Jin, H.; Heller, D. A.; Kim, J.-H.; Strano, M. S. Stochastic Analysis of Stepwise Fluorescence Quenching Reactions on Single-Walled Carbon Nanotubes: Single Molecule Sensors. *Nano Lett.* **2008**, *8*, 4299–4304.

18. Siitonen, A. J.; Tsyboulski, D. A.; Bachilo, S. M.; Weisman, R. B. Surfactant-Dependent Exciton Mobility in Single-Walled Carbon Nanotubes Studied by Single-Molecule Reactions. *Nano Lett.* **2010**, *10*, 1595–1599.

19. Heller, D. A.; Jin, H.; Martinez, B. M.; Patel, D.; Miller, B. M.; Yeung, T.-K.; Jena, P. V.; Hobartner, C.; Ha, T.; Silverman, S. K.; *et al.* Multimodal Optical Sensing and Analyte Specificity Using Single-Walled Carbon Nanotubes. *Nat. Nanotechnol.* **2009**, *4*, 114–120.

20. Georgi, C.; Böhmler, M.; Qian, H.; Novotny, L.; Hartschuh, A. Probing Exciton Propagation and Quenching in Carbon Nanotubes with Near-Field Optical Microscopy. *Phys. Status Solidi B* **2009**, *246*, 2683–2688.

21. Moritsubo, S.; Murai, T.; Shimada, T.; Murakami, Y.; Chiashi, S.; Maruyama, S.; Kato, Y. K. Exciton Diffusion in Air-Suspended Single-Walled Carbon Nanotubes. *Phys. Rev. Lett.* **2010**, *104*, 247402.

22. Berciaud, S.; Cognet, L.; Lounis, B. Luminescence Decay and the Absorption Cross Section of Individual Single-Walled Carbon Nanotubes. *Phys. Rev. Lett.* **2008**, *101*, 077402.

23. Heller, D. A.; Mayrhofer, R. M.; Baik, S.; Grinkova, Y. V.; Usrey, M. L.; Strano, M. S. Concomitant Length and Diameter Separation of Single-Walled Carbon Nanotubes. *J. Am. Chem. Soc.* **2004**, *126*, 14567–14573.

24. Rajan, A.; Strano, M. S.; Heller, D. A.; Hertel, T.; Schulten, K. Length-Dependent Optical Effects in Single Walled Carbon Nanotubes. *J. Phys. Chem. B* **2008**, *112*, 6211–6213.

25. Redner, S. *A Guide to First-Passage Processes*; Cambridge University Press: New York, 2007; pp 255−258.

26. Hartschuh, A.; Qian, H.; Meixner, A. J.; Anderson, N.; Novotny, L. Nanoscale Optical Imaging of Excitons in Single-Walled Carbon Nanotubes. *Nano Lett.* **2005**, *5*, 2310–2313.

27. Qian, H.; Georgi, C.; Anderson, N.; Green, A. A.; Hersam, M. C.; Novotny, L.; Hartschuh, A. Exciton Transfer and Propagation in Carbon Nanotubes Studied by Near-Field Optical Microscopy. *Phys. Status Solidi B* **2008**, *245*, 2243–2246.

28. Cognet, L.; Tsyboulski, D. A.; Weisman, R. B. Subdiffraction Far-Field Imaging of Luminescent Single-Walled Carbon Nanotubes. *Nano Lett.* **2008**, *8*, 749–753.

29. Perebeinos, V.; Tersoff, J.; Avouris, P. Radiative Lifetime of Excitons in Carbon Nanotubes. *Nano Lett.* **2005**, *5*, 2495–2499.

30. Berberan-Santos, M.; Bodunov, E.; Valeur, B. Mathematical Functions for the Analysis of Luminescence Decays with Underlying Distributions 1. Kohlrausch Decay Function (Stretched Exponential). *Chem. Phys.* **2005**, *315*, 171–182.

31. Georgi, C.; Green, A. A.; Hersam, M. C.; Hartschuh, A. Probing Exciton Localization in Single-Walled Carbon Nanotubes Using High-Resolution Near-Field Microscopy. *ACS Nano* **2010**, *4*, 5914–5920.

32. Xiao, Y.-F.; Nhan, T. Q.; Wilson, M. W. B.; Fraser, J. M. Saturation of the Photoluminescence at Few-Exciton Levels in a Single-Walled Carbon Nanotube under Ultrafast Excitation. *Phys. Rev. Lett.* **2010**, *104*, 017401.

33. Lefebvre, J.; Finnie, P.; Homma, Y. Temperature-Dependentcence from Single-Walled Carbon Nanotubes. *Phys. Rev. B* **2004**, *70*, 045419.

34. Ma, Y.-Z.; Graham, M. W.; Fleming, G. R.; Green, A. A.; Hersam, M. C. Ultrafast Exciton Dephasing in Semiconducting Single-Walled Carbon Nanotubes. *Phys. Rev. Lett.* **2008**, *101*, 217402.

35. Mortimer, I. B.; Nicholas, R. J. Role of Bright and Dark Excitons in the Temperature-Dependent Photoluminescence of Carbon Nanotubes. *Phys. Rev. Lett.* **2007**, *98*, 027404.

36. Shaver, J.; Kono, J.; Portugall, O.; Krstić, V.; Rikken, G. L. J. A.; Miyauchi, Y.; Maruyama, S.; Perebeinos, V. Magnetic Brightening of Carbon Nanotube Photoluminescence through Symmetry Breaking. *Nano Lett.* **2007**, *7*, 1851–1855.

37. Pedersen, T. G. Exciton Effects in Carbon Nanotubes. *Carbon* **2004**, *42*, 1007–1010.

38. Strano, M. S.; Huffman, C. B.; Moore, V. C.; O'Connell, M. J.; Haroz, E. H.; Hubbard, J.; Miller, M.; Rialon, K.; Kittrell, C.; Ramesh, S.; *et al.* Reversible, Band-Gap-Selective Protonation of Single-Walled Carbon Nanotubes in Solution. *J. Phys. Chem. B* **2003**, *107*, 6979–6985.

39. Graham, M. W.; Ma, Y.-Z.; Fleming, G. R. Femtosecond Photon Echo Spectroscopy of Semiconducting Single-Walled Carbon Nanotubes. *Nano Lett.* **2008**, *8*, 3936–3941.

40. Miyauchi, Y.; Hirori, H.; Matsuda, K.; Kanemitsu, Y. Radiative Lifetimes and Coherence Lengths of One-Dimensional Excitons in Single-Walled Carbon Nanotubes. *Phys. Rev. B* **2009**, *80*, 081410.

41. Perebeinos, V.; Tersoff, J.; Avouris, P. Scaling of Excitons in Carbon Nanotubes. *Phys. Rev. Lett.* **2004**, *92*, 257402.

42. Pedersen, T. G. Variational Approach to Excitons in Carbon Nanotubes. *Phys. Rev. B* **2003**, *67*, 073401.